Ocean Sci. J. (2011) 46(4):273-288
http://dx.doi.org/10.1007/s12601-011-0021-z

Article

Available online at www.springerlink.com

SpringerLink

Ocean Science Journal

Tidal Transport through the Tsugaru Strait - Part I: Characteristics of the Major Tidal Flow and its Residual Current

Quang-Hung Luu[1,2]*, Kosuke Ito[1,3], Yoichi Ishikawa[1], and Toshiyuki Awaji[1]

[1]*Department of Geophysics, Kyoto University, Kyoto 606-8502, Japan*
[2]*Department of Mathematics, Vietnam National University, Hanoi, Vietnam*
[3]*Department of Atmospheric Sciences, Taiwan National University, Taipei 10617, Taiwan*

Received 19 October 2011; Revised 5 December 2011; Accepted 20 December 2011

Abstract – The potential role of the tide-induced time-mean flow (the tidal residual current) in determining transport through the Tsugaru Strait (located between the East/Japan Sea and the North Pacific) is investigated using a high-resolution numerical barotropic model. The calculated K_1, O_1, M_2, and S_2 tidal fields agree well with available observational records derived from both tide gauge and current meter measurements in the strait and the adjacent seas. The tidal residual current speed reaches 0.3 ms^{-1} in two narrow "neck" areas where topographic sills are located. This result suggests that tides should be taken into account in estimating the long-term water mass and nutrient transport through narrow regions between the East/Japan Sea and the North Pacific. An interesting aspect of the tidal residual current field is the prediction of several active eddy zones in which sequences of eddy triplets develop in the vicinity of capes. Our vorticity analysis reveals that the interplay of topographic effects arising from both the headland and the sill around capes plays a critical role in the formation of these triple eddy patterns.

Key words – Tsugaru Strait, regional tide model, tidal residual current, eddy triplet

1. Introduction

The Tsugaru Strait is located between the two largest Japanese islands, Honshu and Hokkaido. This shallow strait (about 128 m depth on average) is the major conduit for waters moving from the East/Japan Sea to the deep North Pacific. Talley et al. (2006) showed that the waters of the East/Japan Sea are more saline than the North Pacific waters and are cold enough to modify, at least in part, the properties of the dense water in the western North Pacific (Nakamura et al. 2000), namely the North Pacific Intermediate Water. They suggested that the overturning of the North Pacific is indirectly affected by water properties in the East/Japan Sea flowing through the Tsugaru Strait as well as the Soya Strait.

Previous studies clarified that flow through the Tsugaru Strait is characterized by both the Tsugaru Warm Current (hereafter, referred to as TWC) and the tidal current (Onishi et al. 2004). The TWC, a throughflow from the East/Japan Sea to the North Pacific (Fig. 1a), is thought to play a primary role in determining transport through the Tsugaru Strait. The volume of water transported by the TWC varies seasonally from 1.0 Sv to 2.1 Sv (1 Sv = 10^6 m^3s^{-1}) throughout the year and has a mean value of 1.4-1.8 Sv (Toba et al. 1982; Onishi and Ohtani 1997; Ito et al. 2003; Na et al. 2009). The main force driving the TWC is the difference in sea level between the two oceanic basins (Conlon 1981; Toba et al. 1982; Ito et al. 2003).

On the other hand, tidal processes in this region have also received considerable attention. For example, by using a ship-mounted Acoustic Doppler Current Profiler (ADCP), Onishi et al. (2004) reported that the amplitudes of the K_1 and M_2 tidal components at 25 m depth in the central portion of Line F (Fig. 1c), running from Hakodate (Hokkaido Island) to Mutsu Bay (Honshu Island), are both roughly 0.35 ms^{-1}. Off Cape Ohma (Line H in Fig. 1c), the maximum speed of the K_1 tidal current, as derived from a ferry-boat-mounted ADCP measurement, is greater than 1 ms^{-1} (Kuroda et al. 2004). However, the available observations are still too

*Corresponding author. E-mail: luuqh@kugi.kyoto-u.ac.jp

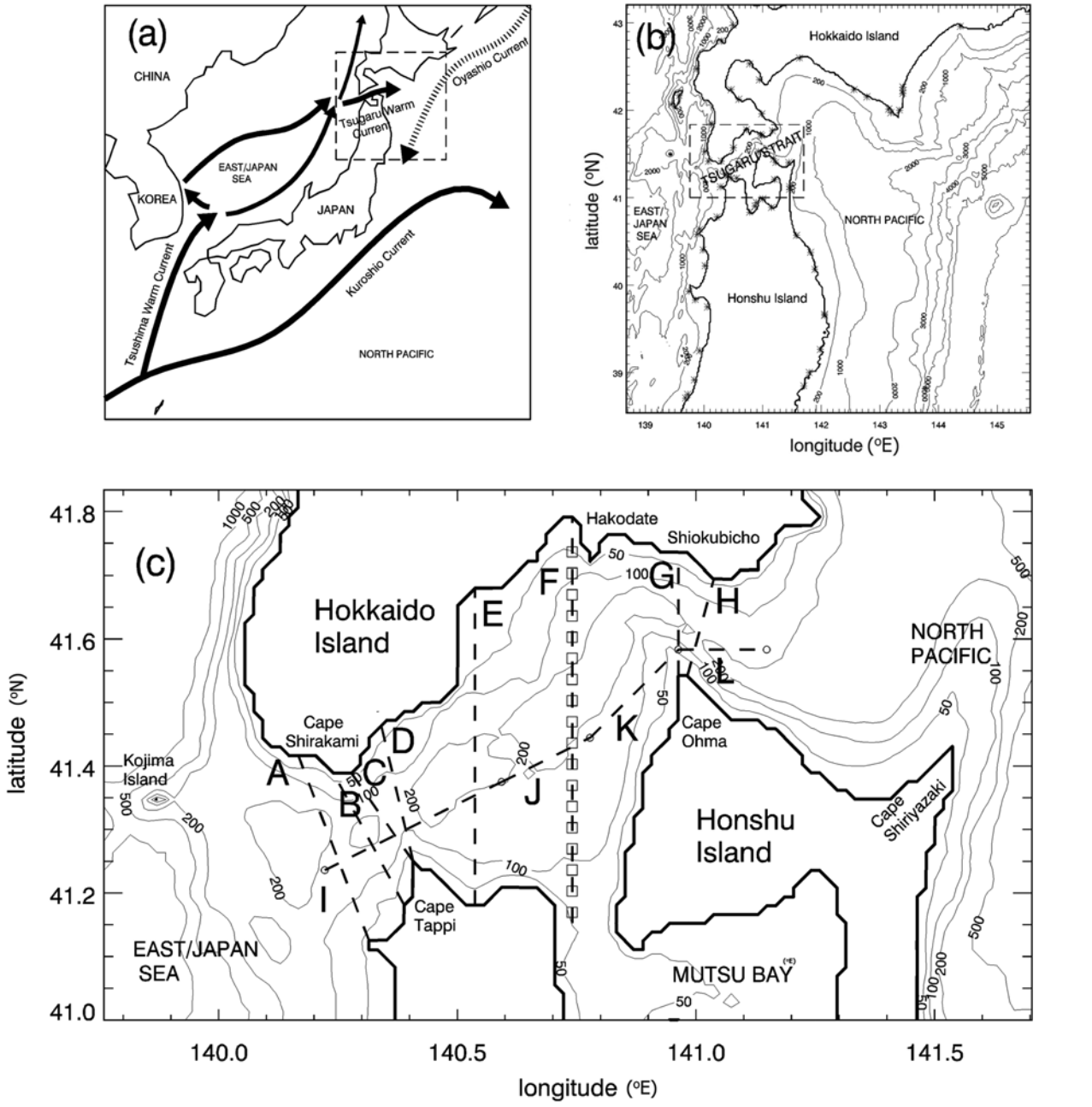

Fig. 1. (a) Schematic view of the model domain. (b) Model domain and topography. (Contours are at 200, 1000, 2000, 3000, 4000, 5000, and 6000 m depths.) Symbols denote the locations of tide gauges from which tidal harmonic constants used by the Japan Coast Guard are derived (1992). (c) Detailed bathymetry in the Tsugaru Strait and locations of the current observation sites obtained by Onishi et al. (2004) (rectangular symbols). (Contours are at 50, 100, 200, 500, and 1000 m depths.) Dashed lines A-L indicate cross sections for estimating the amplitude of tidal volume transport. Open circles denote terminals of along-strait lines

spatially scattered to fully reveal the horizontal tidal structures (Onishi et al. 2004; Na et al. 2009). For this reason, numerical modeling studies have been performed to better understand the physics of tides in the Tsugaru Strait. In particular, Isoda and Baba (1998) developed a two-dimensional numerical model for the K_1 and M_1 tides in the Tsugaru Strait that yielded a current speed of 0.9 ms^{-1} (for the K_1 tide) at both necks of the Tsugaru Strait. They also studied the nonlinear interaction between the tidal current and the TWC with further analysis based on a one-dimensional analytical model.

Although these previous studies revealed several important

features of fundamental tidal process in the Tsugaru Strait, more realistic descriptions of the entire Tsugaru Strait region are required to better understand the dynamic nature of the water mass transport process. In particular, the contribution of tide-induced time-mean flows (hereafter, the tidal residual current) is yet to be clarified in this region. It has long been recognized that the tidal residual current plays an important role in the long-term transport of water, heat, nutrients, sediments, and pollutants in coastal and strait regions (Pingree 1978; Zimmerman 1981; Nihoul and Hecq 1984; Guo et al. 2004; Nakamura et al. 2000; Signell and Haris 2000; Berthot and Pattiaratchi 2006; Li 2006; Burgess et al. 2007; Ro et al. 2007). In fact, one may expect that the tidal residual current is an important potential factor in estimating the long-term transport in the Tsugaru Strait, particularly through narrow areas surrounded by headlands (Awaji et al. 1980; Zimmerman 1981) where tidal currents exhibit considerable speeds. In the Tsugaru Strait, such narrow areas are characterized by the presence of sill-like topographic features as well as headlands. These two physical features have already been identified as major factors in the generation of tidal residual currents (Zimmerman 1981; Robinson 1981; Ridderinkhof 1989).

Against this background, we have performed a numerical investigation of tidal currents in this region as a first step towards the better understanding of transport processes through the Tsugaru Strait. To do so, a tidal simulation was conducted using the Kyoto University Ocean General Circulation Model. Accurate and detailed geographical information has been introduced in order to make realistic tidal predictions. The use of accurate harmonic constants is also an important factor in the reproduction of real conditions. This approach contrasts with the constant values adopted for the harmonic constituents by Isoda and Baba (1998). These improvements enable us to better evaluate the tidal fields and hence the long-term transport as represented by the tidal residual current.

In this study (Part I), our approach focuses on the reproduction of accurate barotropic tide and tidal current fields in the absence of the TWC. Important interactions with the TWC and other baroclinic effects will be discussed in Part II. Our work is primarily a modeling study of a possible role of tidal processes in determining transport through the Tsugaru Strait. Nevertheless, the tide obtained from our numerical model agrees well with data from previous tidal field studies as illustrated below, and this allows us to investigate the potential role of the tidal residual current as a first step.

The main objectives of this paper are (1) to reveal the physical process of tidal elevations and currents in the entire Tsugaru Strait; (2) to evaluate the potential contribution of tidal residual current to the mean transport through the strait; and (3) to understand the dynamic nature of the tidal residual current field in the Tsugaru Strait.

The paper is organized as follows. The numerical model and the settings are described in section 2. Section 3 aims to validate our numerical results with available coastal tide gauge and current measurements. In section 4, the pronounced features of the calculated tides and currents are shown, and section 5 exhibits interesting features present in the tidal residual current and suggests processes that may be responsible for their dynamic nature. We summarize our main findings in section 6.

2. Model Description

The model domain (Fig. 1b) in this study covers a rather broad region from 138°40′E to 145°35′E longitude and from 38°35′N to 43°20′N latitude, in order to better reproduce tidal waves propagating from the North Pacific, which are regarded as the major forcing of tidal motions within the Tsugaru Strait.

The numerical model used in this study is an updated version of that used by Toyoda et al. (2004), a three-dimensional primitive-equation model based on spherical coordinates. It has a horizontal grid spacing of 1/54° ×1/72° and a vertical representation of 78 σ-z hybrid levels. Here, temperature and salinity are set to be constant (hence constant density) in order to focus on the role of the barotropic tide. As a first step toward clarifying the robust role of tides in contributing to throughflow transport, the nonlinear interaction between tidal constituents is not considered in the present study. For this reason, the tidal field is independently calculated for the four major constituents of K_1, O_1, M_2, and S_2 (Onishi et al. 2004), and thus astronomical arguments are neglected as suggested by Schwiderski (1980).

The simulation experiment for each barotropic tide is performed by introducing the tidal potential term into the model equations together with the forcing at the open boundaries. To determine a realistic open boundary condition, we employ the dataset of harmonic constants derived from the NAO.99Jb model (Matsumoto et al. 2000). It is an

improved version of NAO.99b and is constructed by assimilating both TOPEX/POSEIDON altimeter data and coastal tide gauge data at 219 stations around Japan and Korea for 5 years. It provides more accurate harmonic constants than other tide model in the areas adjacent to Japan (Matsumoto et al. 2000). The harmonic constants of NAO.99Jb with a horizontal resolution of 1/12° ×1/12° are smoothly interpolated onto the higher resolution model grids at the open boundary.

The equations for the barotropic mode can be expressed as follows:

$$\frac{\partial \eta}{\partial x} + \frac{1}{a\cos\varphi}\left[\frac{\partial (H+\eta)U}{\partial x} + \frac{\partial (H+\eta)V}{\partial y}\right] = 0 \quad (1)$$

$$\frac{\partial U}{\partial t} - fV = -\frac{g}{a\cos\varphi}\frac{\partial (\alpha\eta - \beta\zeta)}{\partial \varphi} - \frac{\tau_\lambda^b - \tau_\varphi^d}{\rho_0} + X = 0 \quad (2)$$

$$\frac{\partial V}{\partial t} + fU = -\frac{g}{a}\frac{\partial (\alpha\eta - \beta\zeta)}{\partial \varphi} - \frac{\tau_\varphi^b - \tau_\varphi^d}{\rho_0} + Y = 0 \quad (3)$$

where (λ, φ) are latitude and longitude in a spherical coordinate system, respectively. The term t represents time; H, depth; f, the Coriolis parameter; g, gravitational acceleration; a, the earth's radius; ρ_0, the density; and η, the water elevation at the sea surface. The quantities U and V are the vertically averaged horizontal velocity in the λ and φ directions, respectively, whereas X and Y represent the vertically averaged advective and viscous terms (see Appendix A for more detail). The parameters α and β account for the effects of the tidal potentials, earth tide, and loading tide (Schwiderski 1980; Nakamura et al. 2000). We used values of $\alpha = 0.900$ and $\beta = 0.690$ following Schwiderski (1980). The equilibrium tide ζ is expressed as

$$\zeta = k\sin 2\lambda \cos\left(\frac{2\pi}{T}t + \varphi\right) \quad (4)$$

for diurnal and as

$$\zeta = k\cos^2\lambda \cos\left(\frac{2\pi}{T}t + 2\varphi\right) \quad (5)$$

for semidiurnal tides, where T is the tidal period of each constituent. Values of k are taken from Schwiderski (1980) as shown in Table 1. Bottom stresses are expressed as τ_λ^b and τ_φ^b. The magnitudes of these stress terms at the bottom are assumed to be proportional to the flow speed with an inclined angle $\pi + \theta$ to the velocity vector (Weatherly 1972). They are written in the familiar quadratic form as follows:

Table 1. Tidal parameters used in the model, after Schwiderski (1980)

Tide	k (m)	Frequency ($\times 10^{-4}$ cycles/s)
K_1 (diurnal) declination luni-solar	0.141565	0.72921
O_1 (diurnal) principal lunar	0.100514	0.67598
M_2 (semi-diurnal) principal lunar	0.242334	1.40519
S_2 (semi-diurnal) principal solar	0.112841	1.45444

$$\tau_\lambda^b = \rho_0 c_0 (u_b\cos\theta - v_b\sin\theta)\sqrt{u_b^2 + v_b^2} \quad (6)$$

$$\tau_\varphi^b = \rho_0 c_0 (v_b\cos\theta + u_b\sin\theta)\sqrt{u_b^2 + v_b^2} \quad (7)$$

where u_b, v_b are the horizontal velocity components at the lowest model layer. The drag coefficient and angle are set to $c_0 = 1.225\times 10^{-5}$ (m^{-1}) and $\theta = 10^o$, respectively.

In this study, additional dumping terms τ_λ^d and τ_φ^d are introduced because the overestimation of tidal energy is a well-known problem (e.g. Arbic et al. 2004; Schiller 2004). Since a detailed formulation is beyond the scope of this study, we instead define these terms for practical use in a fashion similar to Schiller and Fiedler (2007). According to Döös et al. (2004), we have carried out several sensitivity experiments, and found that the following dumping terms in the barotropic equation yield the smallest root mean square (RMS) errors for both elevation and current:

$$\tau_\lambda^d = \rho_0 (c_1 + c_2\sqrt{U^2 + V^2})U \quad (8)$$

$$\tau_\lambda^d = \rho_0 (c_1 + c_2\sqrt{U^2 + V^2})V \quad (9)$$

where the parameters $c_1 = 1\times 10^{-5}$ (s^{-1}) and $c_1 = 5\times 10^{-6}$ (m^{-1}) are determined by trial and error.

The boundary conditions are set as follows. At the lateral coastal boundary, a no-slip condition is used. At lateral open boundaries, the sea-level elevation is imposed using the results of NAO.99Jb, with the exceptions of the Oshika Peninsula, Awashima Island, Cape Kamui, and Cape Shirepa, where elevation is given directly from tide gauge observations near the open boundaries. At the sea surface, the vertical gradient of velocity is zero. The bathymetry used in this study is from the 30-s resolution grid (JTOPO30) for regions around Japan edited by the Marine Information Research Center of the Japan Hydraulic Association. A better representation of the tidal field is anticipated from the use of this highly sophisticated bottom topography. The bathymetry is smoothly interpolated on the corresponding model grid points by the spline method.

The numerical calculation for each tidal constituent starts from a rest state, and continues through a time-integration of 37 tidal cycles by which time the final cycle is almost in an equilibrium steady state. The results of each final cycle are then used for our analysis.

3. Validation of Computed Tides

Comparison with tide gauge data

The harmonic constants at 67 widely spread coastal tide gauge stations established around this region by the Japan Coast Guard (1992) are used to evaluate our model's performance. The location of each tide gauge is adjusted to its closest model grid point with an accuracy of 1/60°×1/60° (Fig. 1b). Comparison between the calculated and observed amplitudes and phases are shown in Fig. 2.

The RMS errors between the sea level elevation obtained from the tide gauge data and that from the model results are evaluated using the following formula as in Hatayama et al. (1996) and Nakamura et al. (2000):

$$\mathrm{RMS} = \frac{1}{N}\sum_{n=1}^{N}\left\{\frac{1}{T}\int_0^T\left[A_n^M\cos\left(\frac{2\pi}{T}t+\phi_n^M\right)-A_n^O\cos\left(\frac{2\pi}{T}t+\phi_n^O\right)\right]^2 dt\right\}^{1/2} \quad (10)$$

where N is the total number of tide gauge observations. Here, A and ϕ are the amplitude and phase, respectively. The superscripts M and O denote the calculated and observed values, respectively. The RMS errors for K_1, O_1, M_2, and S_2 are 0.0291 m, 0.0171 m, 0.0193 m, and 0.0089 m, respectively. These values indicate that all constituents are well reproduced in the region of the Tsugaru Strait and its adjacent seas.

For the dominant K_1 constituent (in terms of maximum speed), the correlation coefficients are high (0.966 for amplitude and 0.961 for phase), and they are also high for the O_1 constituent (0.954 for amplitude and 0.933 for phase). Correlation coefficients for the amplitudes of the semidiurnal tides are high, 0.973 and 0.979 for M_2 and S_2, respectively. The low correlation coefficients for M_2 and S_2 phase, as seen in Figs. 2f and 2h, are due to the rapid propagation of semidiurnal tides throughout the short length of the Tsugaru Strait. In this case, a more appropriate comparison may be made by rewriting the tidal constants as: $AC_n = A_n \cos\phi$, $AS_n = A_n \sin\phi$. Hence, the RMS in Eq. (10) can be simplified as follows:

$$\mathrm{RMS}=\frac{1}{N}\sum_{n=1}^{N}\left\{\frac{1}{2}\left[(AC_n^M-AC_n^O)+(AS_n^M-AC_n^O)\right]\right\}^{1/2} \quad (11)$$

The new RMS errors are reduced somewhat to 0.0156 m and 0.0086 m for M_2 and S_2, respectively. Our calculation is

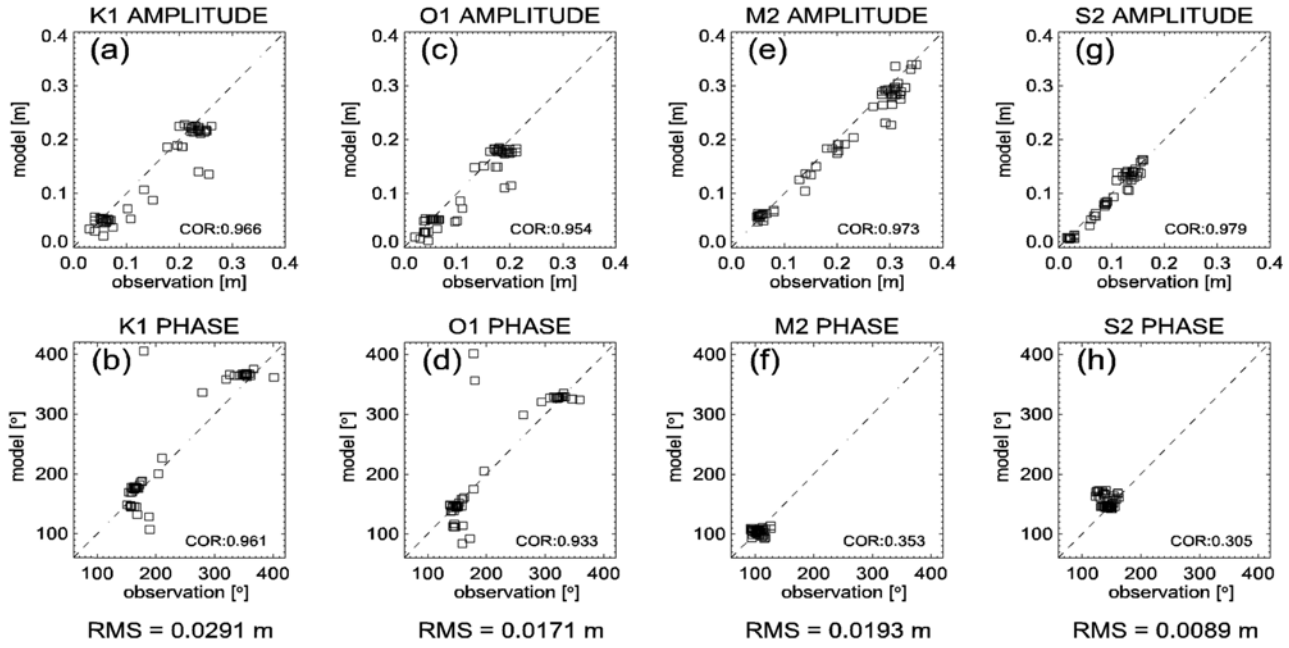

Fig. 2. Comparison of amplitudes and phases of K_1, O_1, M_2, and S_2 tides between simulated results and observational data at 67 coastal tide gauge stations

thus successful in representing the dominant barotropic tidal components in the Tsugaru Strait.

Of 67 stations, sea-level amplitudes at 5 stations (Tappi, TappiSaki, Wakimoto, SiokubiMisaki, and Yoshioka in Fig. 1b) located at the western and the eastern necks within the strait are slightly underestimated. This may be due to the nonlinear interaction between the tidal current and the TWC (Isoda and Baba 1998).

Comparison with current measurements

In addition to the tide gauge data, we compare the calculated volume transport across the north-south cross section of Line F (see Fig. 1c) with that from the long-term tide current measurement made by Onishi et al. (2004). Here, the volume transport amplitude in the numerical model is defined as the maximum value of the calculated volume transport across the corresponding line during one tidal cycle. The calculated extremes of volume transport are 0.38 Sv for M_2, 0.19 Sv for S_2, 0.83 Sv for K_1, and 0.75 Sv for O_1, while the results shown in Onishi et al. (2004) are 0.52 Sv for M_2, 0.24 Sv for S_2, 0.72 Sv for K_1, and 0.60 Sv for O_1. Thus, our model reasonably captures the observed features of volume transport for each tide.

The close similarities between our results and observations of coamplitude, cophase, and volume transport encourage us to conduct further investigations and analyses. However, more elaborate treatments such as the inclusion of baroclinic tides and nonlinear interactions with the TWC are required for further improvements. These aspects will be addressed in Part II.

4. Features of the Tidal Current Fields

Tidal elevations

The spatial distribution of the calculated coamplitude and cophase lines for K_1, O_1, M_2, and S_2 tides are shown in Fig. 3, which indicates that M_2 is the largest constituent with an amplitude of 0.07 m on the western side of the strait and up to 0.30 m on the eastern side. This large difference between both ends of the strait results from the difference in tidal regimes between the East/Japan Sea and the North Pacific. From west to east the amplitude of M_2 increases gradually across the strait. The cophase lines of M_2 vary between about 90°-120° within the strait. This is consistent with Onishi and Ohtani (1997), where the M_2 tide was found to nearly co-oscillate along the entire strait as its wave arrives at both ends almost simultaneously. The basic characteristics of S_2 are the same as those of M_2, although the magnitude of the coamplitude is smaller. The S_2 amplitude increases gradually from 0.02 m on the East/Japan Sea side to 0.14 m on the North Pacific side, while its cophase lines vary between about 140°-170°.

The sea-level amplitude of the largest diurnal constituent, K_1, decreases toward the east from 0.04 m to 0.02 m and then increases to up to 0.21 m around the eastern end. The coamplitude lines in the middle of the strait are distributed in parallel to the strait, in contrast to those of M_2 and S_2. This implies a strong effect of swift diurnal currents on the elevation through the curved tidal stream (Ogura 1932). The cophase lines of the K_1 tide vary locally in the strait. In particular, the amphidromic node of the coamplitude lines around 41°35′N and 140°18′E is a distinguishing feature. Compared to that of K_1, the coamplitude of O_1 is smaller (from 0.04 m to 0.17 m). As in the case of K_1, an amphidromic node appears around 41°30′N, 140°20′E.

The tidal form factor, defined here as the ratio of sea-level amplitude of the semidiurnal tide to that of the diurnal tide (Pugh 1987), is represented in Fig. 4, which shows that the sea-level amplitude of the semidiurnal constituent is dominant in the strait, especially in Mutsu Bay. These results are consistent with previous reports (Isoda and Baba 1998; Onishi et al. 2004).

Tidal current

In Fig. 5, the tidal ellipses of representative diurnal and semidiurnal tides illustrate the larger tidal current speeds of the diurnal constituents as compared with the semidiurnal terms, while the opposite relation holds for sea-level amplitude (i.e. semidiurnal > diurnal) as described in Odamaki (1984). The major axis of the ellipse is roughly directed along the strait and the peak values of tidal current speed occur at the narrow eastern and western necks of the strait. The K_1 tide has the strongest tidal current amplitude, up to 0.9 ms^{-1} in the central portion of the eastern neck (between Cape Ohma and Shiokubucho) and up to about 0.8 ms^{-1} in the central portion of the western neck (between Cape Tappi and Cape Shirakami), while the speed is less than 0.01 ms^{-1} outside the strait in both the East/Japan Sea and the North Pacific. The O_1 tide is the second largest constituent in terms of tidal current amplitude with a maximum speed of 0.75 ms^{-1}. The amplitudes for both M_2 and S_2 are in the range 0.2-0.3 ms^{-1}, and are thus much smaller than these of K_1.

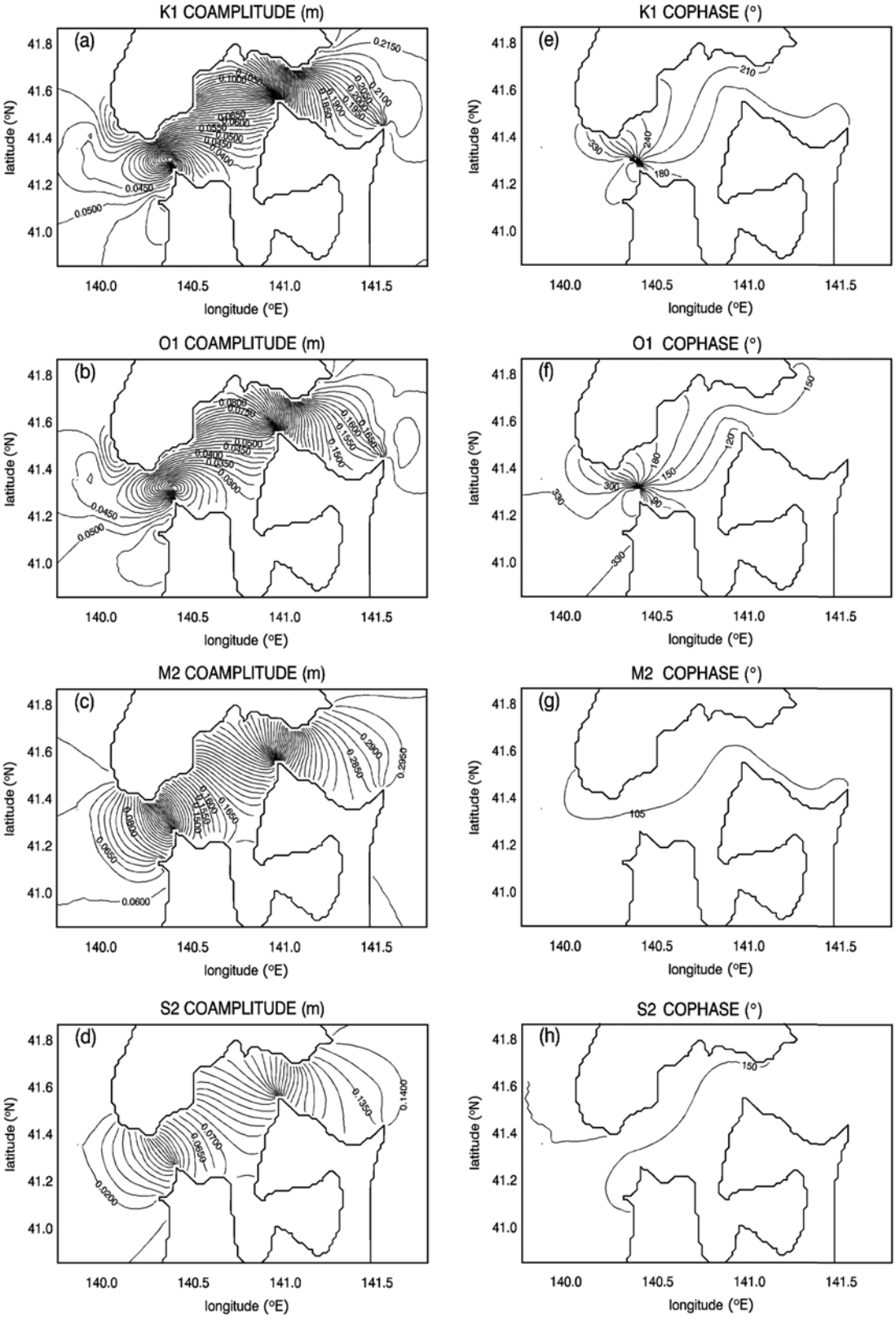

Fig. 3. Left panels (a), (b), (c), (d) depict the calculated coamplitude lines of tidal elevation (in m) for K_1, O_1, M_2, and S_2, respectively. Right panels (e), (f), (g), (h) depict the calculated cophase lines of tidal elevation (in degrees) for K_1, O_1, M_2, and S_2, respectively. The contour intervals for coamplitude are 0.0025 m, and for cophase are 15°

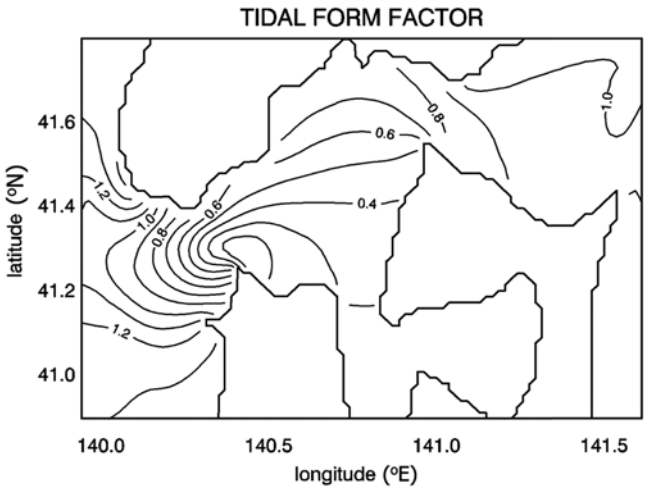

Fig. 4. Form factor distribution in the Tsugaru Strait. The contour interval is 0.1

The temporal maximum values of computed tidal volume transports across eight sections in the strait (see Line A-H in Fig. 1c) are shown in Table 2. The peak value of time-varying K_1 transport is quite large (over 0.9 Sv), comparable to the TWC transport, which has an annual average of about 1.5 Sv (Ito et al. 2003; Na et al. 2009). Therefore, tide-induced transport is likely to be important in our understanding of the long-term water mass and nutrient transport through the Tsugaru Strait. In addition, it is also a key factor in determining the water exchange profile across the strait (Nakamura et al. 2000).

5. Tidal Residual Current

Tidal residual field and associated transport

In this section, we describe the residual current field that we identify as having a major influence on long-term transport.

The calculated residual currents of the K_1, O_1, and M_2 cases are displayed in Fig. 6. The residual current of the S_2 component is not shown here because its maximum speed is smaller than 0.01 ms^{-1}. The result of Fig. 6 clearly shows that the residual flow field is mainly dominated by diurnal tides in the strait. Of these, the K_1 current is the largest with a peak value of 0.15 ms^{-1} (0.12 ms^{-1}) near Cape Ohma (Cape Tappi). Those associated with O_1 reach maximum values of 0.12 ms^{-1} and 0.09 ms^{-1} around the two capes, respectively. The residual current speed of the K_1 tide is about four times larger than that of M_2. This result agrees with the work of

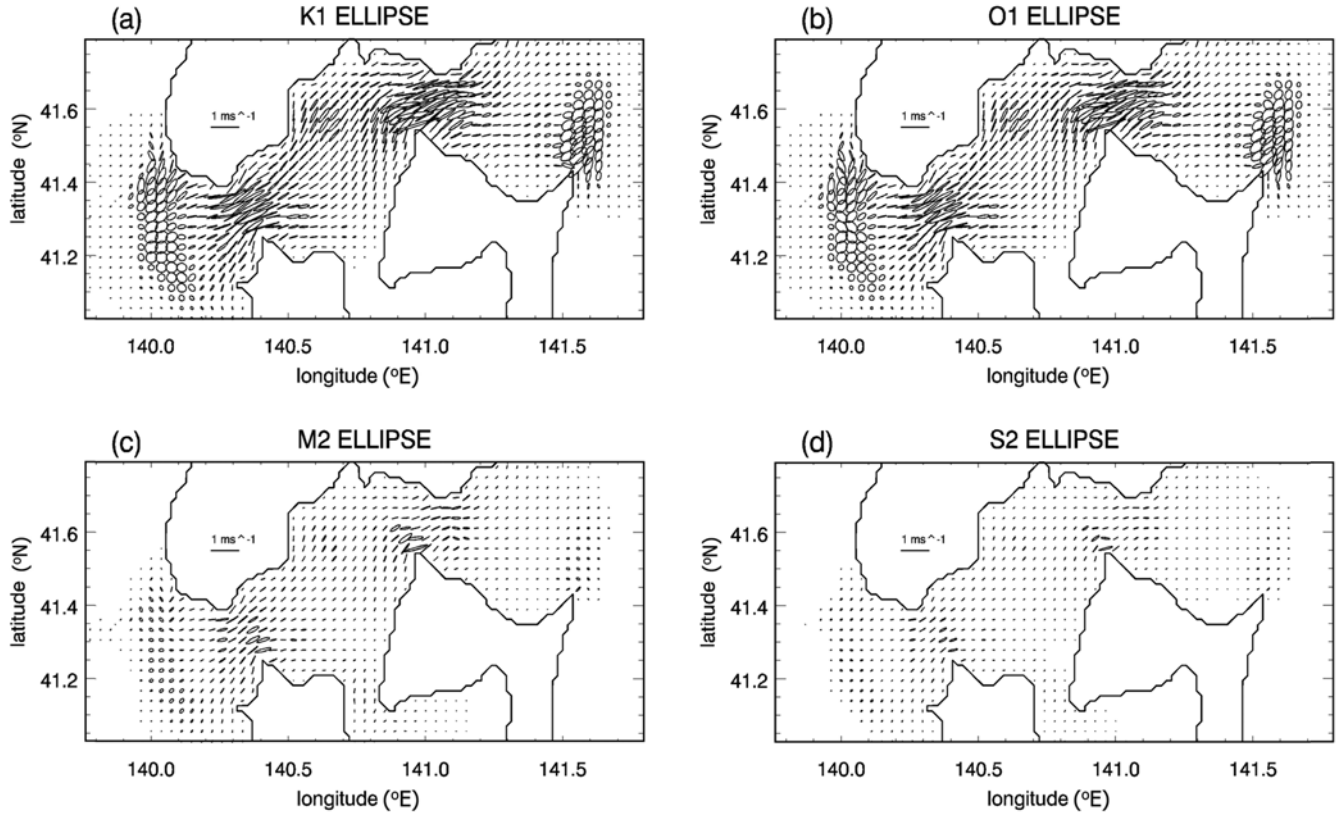

Fig. 5. Calculated tidal ellipses for (a) K_1 tide (b) O_1 tide, (c) M_2 tide, and (d) S_2 tide

Table 2. Temporal extremes of volume transport (in Sv) during one tidal cycle where the velocity is normal to selected sections in between the Tsugaru Strait (as described in Fig. 1c)

Tide	K_1		O_1		M_2		S_2	
Cross-strait transport	min	max	min	max	min	max	min	max
Line A	1.077	-1.065	0.968	-0.955	0.548	-0.545	0.272	-0.273
Line B	0.861	-0.840	0.776	-0.757	0.441	-0.433	0.220	-0.219
Line C	0.933	-0.904	0.839	-0.811	0.471	-0.459	0.232	-0.230
Line D	0.763	-0.742	0.687	-0.668	0.386	-0.376	0.191	-0.189
Line E	0.853	-0.842	0.768	-0.758	0.423	-0.415	0.210	-0.209
Line F	0.831	-0.821	0.750	-0.740	0.385	-0.375	0.192	-0.191
Line G	0.807	-0.816	0.730	-0.737	0.336	-0.330	0.170	-0.170
Line H	0.796	-0.780	0.719	-0.705	0.324	-0.315	0.163	-0.162
Line I	0.138	-0.174	0.132	-0.165	0.058	-0.063	0.029	-0.030
Line J	0.175	-0.166	0.156	-0.147	0.116	-0.115	0.056	-0.056
Line K	0.067	-0.091	0.060	-0.082	0.026	-0.030	0.013	-0.014
Line L	0.358	-0.330	0.327	-0.304	0.124	-0.121	0.063	-0.062

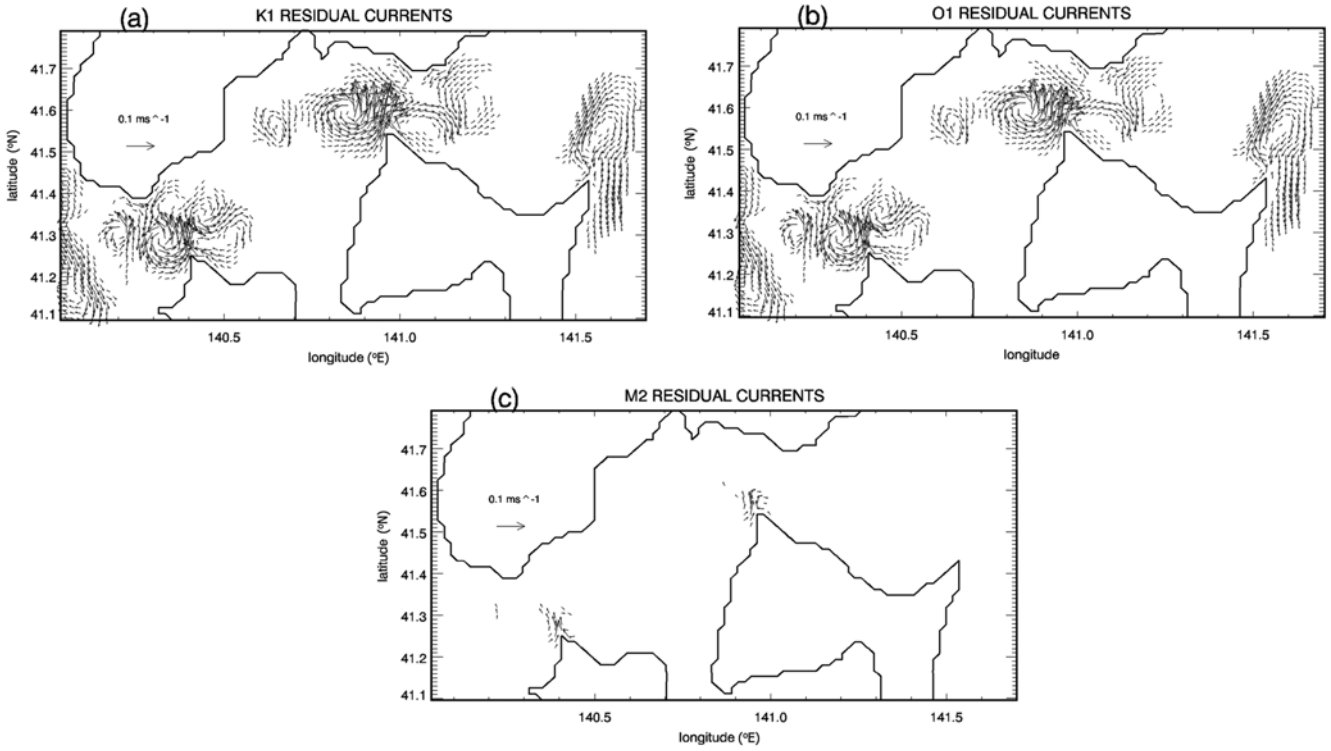

Fig. 6. Time-averaged tidal residual currents (in ms^{-1}) in the Tsugaru Strait for (a) K_1 tide (b) O_1 tide, and (c) M_2 tide. Values smaller than 0.01 ms^{-1} are omitted

Yasuda (1980), who pointed out that the magnitude of the tidal residual current is roughly proportional to the square of the tidal current amplitude. The tidal residual current speed reaches up to 0.3 ms^{-1} (0.27 ms^{-1}) around Cape Ohma (Cape Tappi), which corresponds to about 14% (20%) of the local TWC speed. Figure 7a shows the detailed distribution of tidal residual velocity around the eastern entrance of the Tsugaru Strait and includes observations regarding the intrusion of the southward-flowing coastal Oyashio Current water into the strait, taken from satellite-derived sea surface temperature (SST) images (Fig. 7b). Although the intrusion-like SST distribution could be induced by wind or local cooling effects, the tide-induced residual current pattern is consistent with the spatial distribution of an intruding

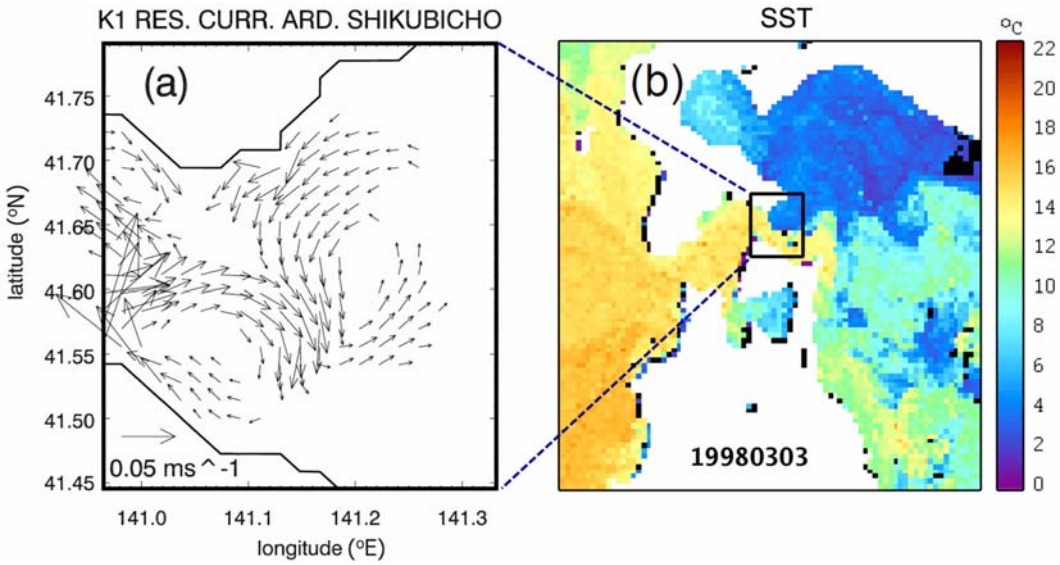

Fig. 7. (a) K_1 tidal residual current around Shiokubicho at the eastern entrance of the Tsugaru Strait. (b) Sea surface temperature image for the occasional westward intrusion of the coastal Oyashio Current water into the northern part of the strait in early March 1998 (NOAA/AVHRR Sea Surface Temperature processed by the Laboratory of Satellite Oceanography of Hokkaido University at http://odyssey.fish.hokudai.ac.jp/AVHRR/). The color bar shows temperature ranges. The cool water of the coastal Oyashio Current is shown in blue

coastal Oyashio Current. These facts suggest that tides likely affect long-term transport and mixing near these capes.

In fact, the tidal residual current fields around these two capes are characterized by intense eddies with diameters of approximately 8-20 km (Fig. 8). Around Cape Tappi, one distinct cyclonic eddy is observed on the left-hand side of the cape, an anticyclonic eddy forms near the coast, and a second cyclonic eddy develops offshore on the right-hand side of the cape. A similar feature is observed around Cape Ohma and Cape Shirakami. To our knowledge, such triple eddy patterns associated with barotropic tidal currents have not yet been reported and thus the physics of these is an interesting aspect of coastal oceanography. Therefore, we conduct a vorticity analysis in the next subsection in order to understand the physical processes involved.

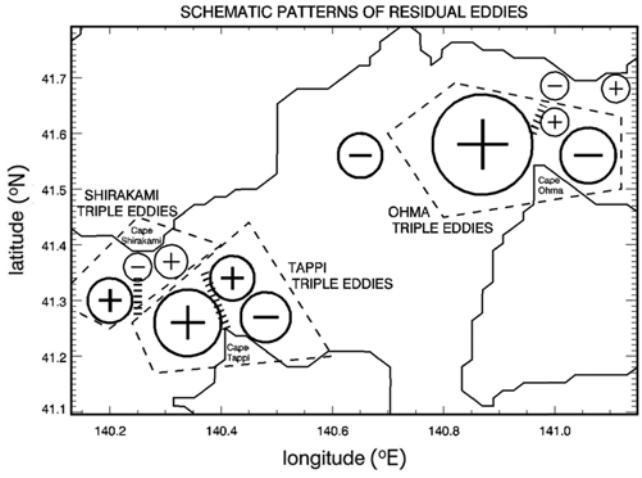

Fig. 8. Schematic patterns of tidal residual eddies in the Tsugaru Strait. Circles with plus (+) and minus (-) signs indicate cyclonic and anticyclonic eddies, respectively. Thick circles imply clearer patterns. "Zebra-crossing" lines (large dashed lines) show the locations of the sills

Formation process of eddy triplets

In general, the major factors involved in the generation of tide-induced residual eddies are thought to be coastal irregularities and/or bathymetric changes (Tee 1977; Zimmerman 1981; Robinson 1981; Ridderinkhof 1989). Previous studies (e.g. Zimmerman 1979; Onishi 1977; Maddock and Pingree 1978; Pingree and Maddock 1979; Signell and Harris 2000) have shown that asymmetric pairs of anticyclonic and cyclonic eddies can be generated on both sides of a headland by oscillatory tidal flow. On the other hand, Robinson (1981) and Maze et al. (1998) indicated that a cyclonic (anticyclonic) eddy can be formed as water moves from deep (shallow) to shallow (deep) regions via stretching and squeezing on the *f*-plane. In the Tsugaru Strait, distinct sill-like bottom topographic features and headland-like coastal protrusions exist. Such topographic features could be responsible for

the unique triple eddy patterns forming offshore from Cape Tappi, Cape Shirakami, and Cape Ohma.

In order to specify the formation process of the eddy triplet, we first examine temporal changes of a relative vorticity field in the dominant K_1 case. Here, relative vorticity is defined as the vertically averaged vertical vorticity as

$$\omega = \frac{1}{a\cos\varphi}\frac{\partial V}{\partial\lambda} - \frac{1}{a}\frac{\partial U}{\partial\varphi} \tag{12}$$

Figure 9 depicts the time series of relative vorticity around Cape Tappi. Positive relative vorticity appears around Cape Tappi between 2 hours to 13 hours from low tide, while negative relative vorticity is seen near the coast from 14 hours to 1 hours (in the next cycle). The time evolution of vorticity around Cape Ohma is analogous (not shown).

To understand the physical process of the relative vorticity change, we evaluate the major terms of the residual vorticity equation as reported in previous studies (Ridderinkhof 1989; Hatayama et al. 1996; Park and Wang 2000).

$$(a) = -\overline{\frac{U}{a\cos\varphi}\frac{\partial\omega}{\partial\lambda} - \frac{V}{a}\frac{\partial\omega}{\partial\varphi}} \tag{13}$$

$$(b) = \overline{\frac{f+\omega}{H+\eta}\frac{d(H+\eta)}{dt}} \tag{14}$$

$$(c) = \overline{c_2\left(\frac{V}{a\cos\varphi\partial\lambda}\frac{\partial}{\partial\lambda} - \frac{U}{a}\frac{\partial}{\partial\varphi}\right)\sqrt{U^2+V^2}} + \overline{c_0\left(\frac{v_b}{a\cos\varphi\partial\lambda}\frac{\partial}{\partial\lambda} - \frac{u_b}{a}\frac{\partial}{\partial\varphi}\right)\sqrt{u_b^2+v_b^2}} + (c_1 + c_2\sqrt{U^2+V^2})\omega$$

$$c_0\sqrt{u_b^2+v_b^2}\left(\frac{V}{a\cos\varphi\partial\lambda}\frac{\partial v_b}{\partial\lambda} - \frac{1}{a}\frac{\partial u_b}{\partial\varphi}\right) \tag{15}$$

where the overbars denote time-averages over one tidal cycle, Eq. (13) gives the advection of vorticity, Eq. (14) represents the vorticity change due to vertical squeezing or stretching of fluid parcels induced by bathymetric changes (Robinson 1981; Cushman-Roisin 1994), and Eq. (15) expresses the vorticity associated with bottom friction. Note that the magnitudes of other terms are smaller than these major terms and their net is approximately balanced in most areas.

Figure 10 shows the spatial distribution of each major term around Cape Tappi in association with the bathymetry.

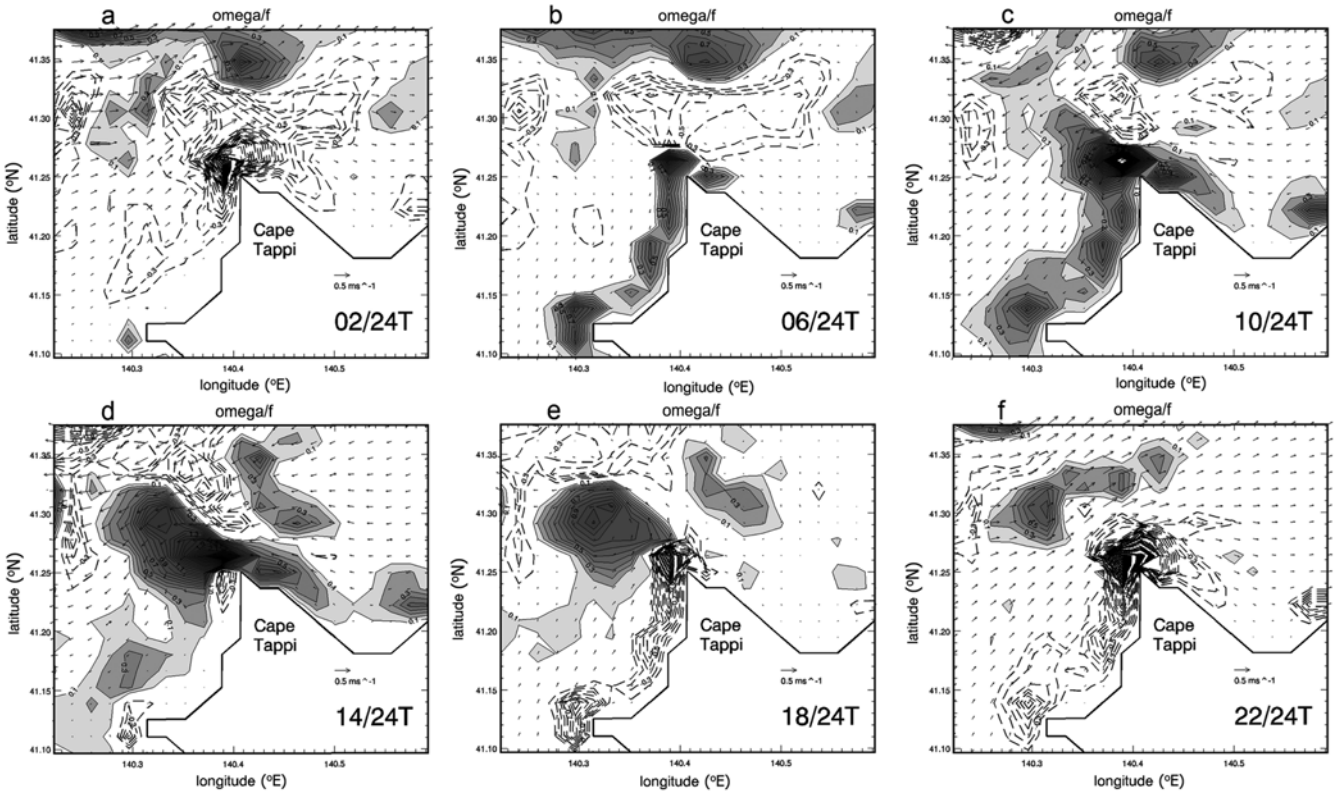

Fig. 9. Temporal changes in the relative vorticity of K_1 with respect to the Coriolis parameter in the Tsugaru Strait during one cycle. The contour interval is 0.1. Shading indicates positive vorticity area, and dashed lines represent negative vorticity

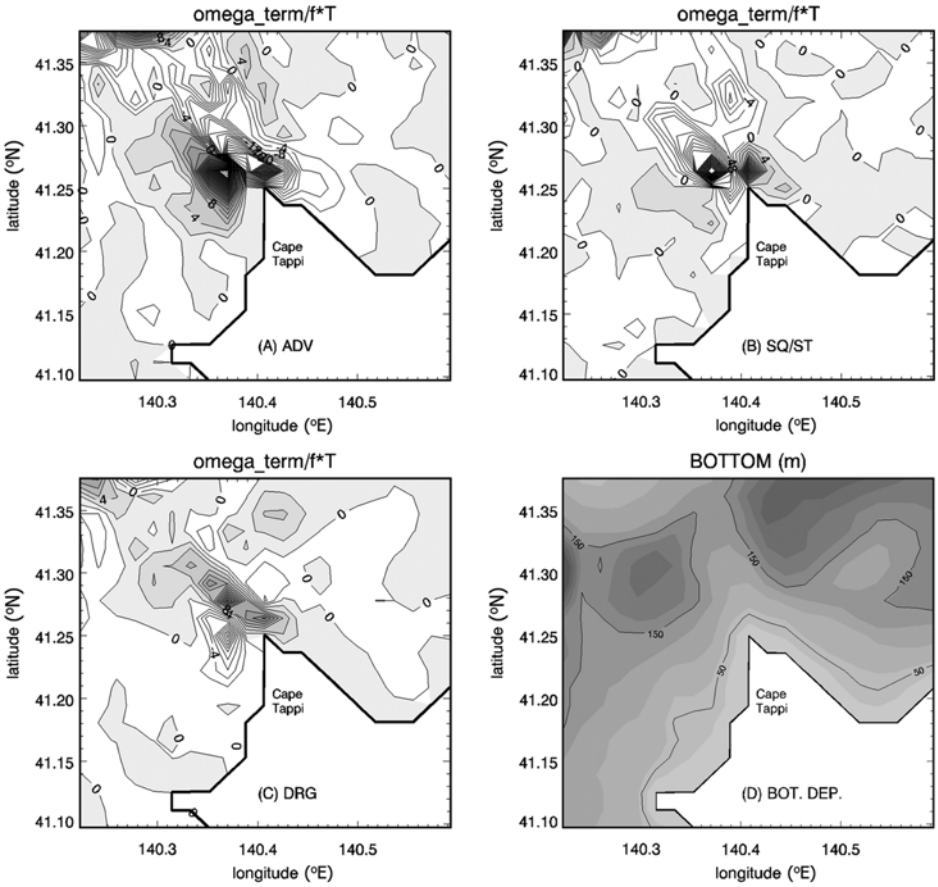

Fig. 10. Time-average of major terms in the vorticity equation. (a) Advection of vorticity. (b) Conservation of potential vorticity when fluid columns spin up or down by squeezing/stretching. (c) Vorticity associated with bottom friction. The contour interval is 2. Shading represents a positive residual area. (d) Isobath contours (in m). Darker shade indicates deeper bathymetry

It reveals that the major term responsible for the formation of residual eddies near Cape Tappi is the vorticity advection (a), as a cyclonic eddy forms on the left-hand side and an anticyclonic eddy develops on the right-hand side. On the other hand, vorticity change arising from vertical squeezing or stretching of fluid parcels induced by a sill (b) is mainly attributed to the generation of a symmetric pair of cyclonic eddies over the sill. Residual vorticity associated with bottom friction (c) is significant in shallow areas, for example over sills (Fig. 10c), but it is smaller than the terms (a) and (b) which contribute mainly to the formation of eddy triplets in offshore regions. These results are consistent with previous generation theories and field studies for headland residual eddies (Zimmerman 1979; Imasato 1983; Signell and Harris 2000) and sill-induced residual eddies (Robinson 1981; Maze et al. 1998; Nakamura et al. 2000), respectively.

From the above results, the formation of a triple residual eddy pattern off Cape Tappi (Fig. 11) is likely to be explained by the interplay of topographic effects arising from both the headland and the sill present around the cape as follows. Positive and negative vorticities are generated on the left-hand and right-hand sides around the cape due to the headland effect, while the sill topography extending offshore induces a relatively large scale positive vorticity on both sides. As a result, the net vorticity field can be characterized by a unique eddy triplet formation near Cape Tappi. This is an interesting feature of the tidal residual flow arising from the co-existence of both headland and sill topography, though the observational support is left for future work and thus the present study is solely a model simulation.

Finally, to confirm our proposed process for the eddy triplet off Cape Tappi, we conduct other experiments referred to as EXP_FBM and EXP_FB250 in which bottom

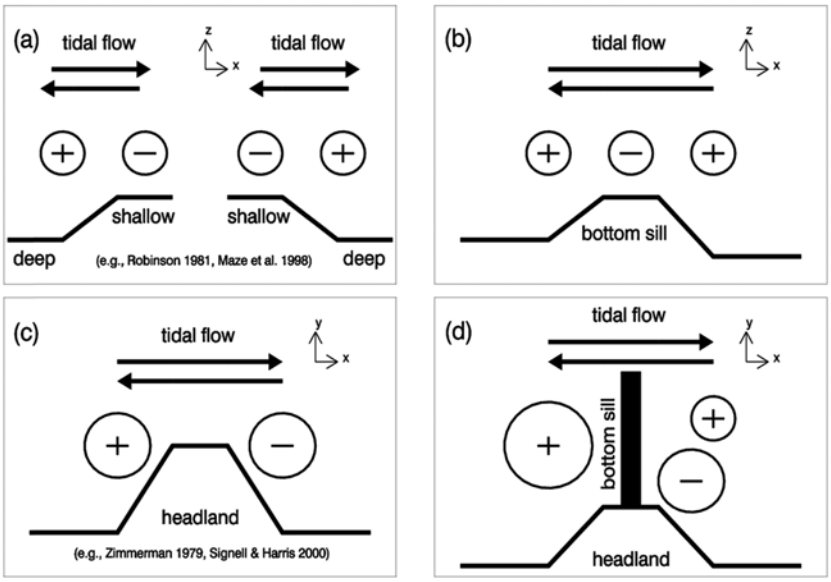

Fig. 11. Schematic illustration of the formation mechanism for triple eddy patterns. (a) Vorticity generation over a slope due to bottom friction. (b) Generation of positive vorticity on both sides of the sill. (c) Vorticity generated around a headland. (d) Triple eddy formation by combined effects of the headland and sill for a sill located at the tip of headland

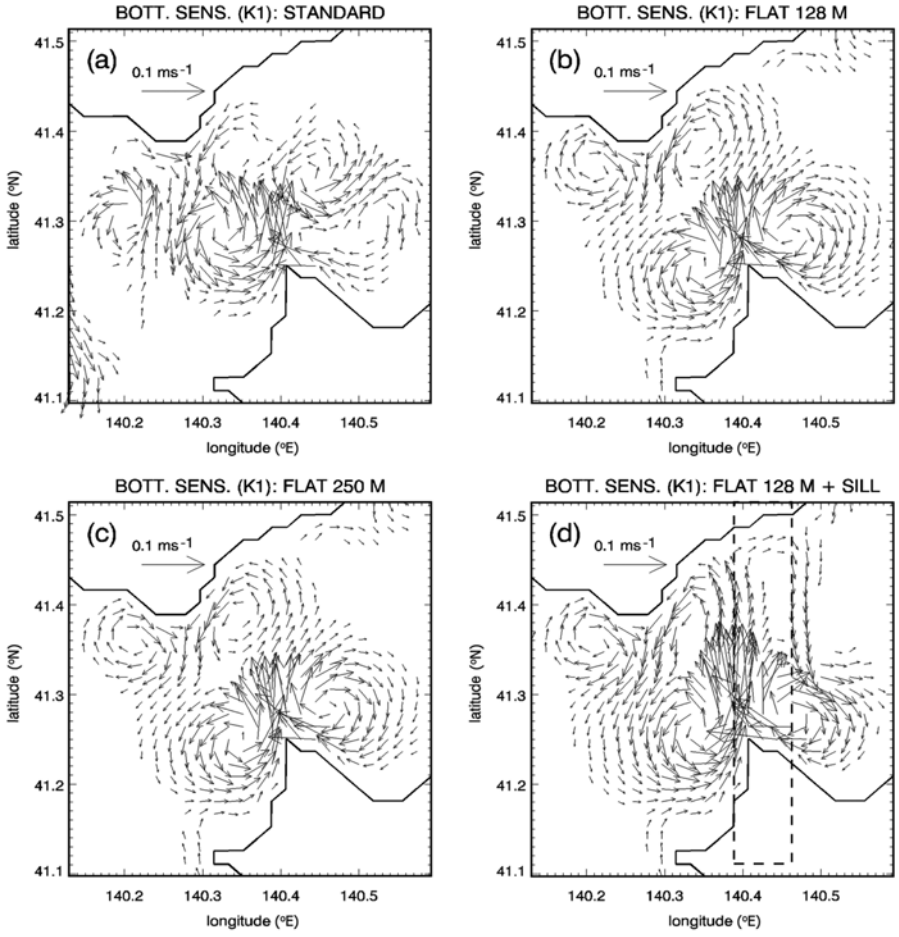

Fig. 12. Time-averaged K_1 residual flow in the Tsugaru Strait for (a) EXP_STD: original case, (b) EXP_FBM: flat bottom using average depth of 128 m, (c) EXP_FB250: flat bottom with a depth of 250 m, and (d) EXP_FB128S: flat bottom with a depth of 128 m with a 100-m sill (shown by dashed rectangular lines)

topography in the Tsugaru Strait region is set to be flat with constant depths of 128 m and 250 m, respectively. We refer to the original calculation as EXP_STD. Figure 12 clearly shows that the headland effect contributes to the generation of only two eddies around the cape and that these are clearly symmetric. This fact also suggests that the presence of sill topography extending offshore is a crucial factor for eddy triplet formation and for the asymmetric pattern revealed in EXP_STD. An additional experiment EXP_FB128S for flat bottom topography with a constant depth of 128 m except for the area along the sill (at a depth of 100 m) confirms the presence of the triple eddy pattern.

6. Summary and Discussion

By incorporating tidal effects into a high-resolution ocean model, we have investigated the barotropic tidal field structure around the Tsugaru Strait and the potential role of the tidal residual flow on long-term transport between the East/Japan Sea and the North Pacific. In spite of our simple assumptions of uniform water temperature and salinity, the calculated results agree well with existing tide gauge and current measurements, and represent an advance on previous studies. These improvements are due to an elaborate treatment of updated tidal harmonic constants and to the use of a sophisticated bathymetric dataset.

The new model gives us an improved description of the tidal effect on water transport and its spatial variability in the Tsugaru Strait. For example, the sea-level amplitude of the semidiurnal tide is larger than that of the diurnal tide, whereas the current amplitude of the diurnal component is larger (0.9 ms^{-1}) than that of the semidiurnal component (0.3 ms^{-1}). In addition, an amphidromic node appears at the western neck of the strait for the diurnal component. These results are consistent with previous findings. The swift K_1 current leads to the considerable temporal maximum volume transport of over 0.9 Sv, which suggests the importance of tidal effects to our understanding of the long-term transport between the strait, particularly when considered alongside TWC.

In order to evaluate the tidal effect on long-term transport, tidal residual currents are calculated for the first time in the Tsugaru Strait. We find that the residual flow field exhibits intense eddy formations with net speeds of 0.3 ms^{-1} on the left-hand sides of Cape Tappi and Cape Ohma on the Honshu coast. The tide-induced cross-strait velocity along Line C reaches up to 20% of that delivered by the TWC, suggesting the potential impact of tidal activity on the long-term transport.

Our simulation reveals the interesting result that the tidal residual current field is characterized by a basic eddy triplet around Cape Tappi, Cape Shirakami, and Cape Ohma, where a strong cyclonic eddy forms on the left-hand side, and anticyclonic and cyclonic eddies develop on the right-hand side. The term balance analysis of the vorticity equation indicates that this triple eddy pattern (shown in Fig. 8) can be interpreted as an interplay of the headland and sill-like topographic effects: Positive and negative zones of vorticity are generated on the left-hand and right-hand sides of the headland, respectively, while symmetrical twin zones of positive vorticity are generated by potential vorticity conservation due to the presence of the sill extending offshore.

Several gross simplifications have been used in the present study. In particular, we highlight the assumptions of uniform temperature and salinity (and thus we neglect baroclinic tidal effects) as well as the absence of the TWC. Indeed, the interplay with the TWC is an important aspect of the current field, and this will be described in the accompanying paper (Part II).

Although many types of eddy pattern have already been reported in previous field studies, the tide-induced triple eddy pattern in this study has not yet been presented. The observational support is left for future work and hence our work is primarily a modeling study of a possible role of tidal processes in transport through the Tsugaru Strait. Nevertheless, this study suggests the potentially important role of the tide on temporal and long-term transport along the Tsugaru Strait, and thereby contributes to a better understanding of the dynamic nature of tidal processes in the Tsugaru Strait.

Acknowledgements

We wish to thank Dr. J. P. Matthews and Prof. K. Akitomo for critically reading the manuscript and for providing useful comments. We also thank T. In for providing data relating to the TWC and Dr. A. Sepulveda for sharing the harmonic analysis algorithm. Thanks are extended to two anonymous reviewers for their valuable suggestions. NOAA/AVHRR Sea Surface Temperature satellite images were provided by the Laboratory of Satellite Oceanography of Hokkaido University. This study was supported partly by the Hakodate Marine Bio Cluster. Numerical calculations

were done at the Academic Center for Computing and Media Studies of Kyoto University.

References

Arbic BK, Garner ST, Hallberg RW, Simmons HL (2004) The accuracy of surface elevations in forward global barotropic and baroclinic tide models. Deep-Sea Res II **51**:3069-3101

Awaji T, Imasato N, Kunishi H (1980) Tidal exchange through a strait: a numerical experiment using a simple model basin. J Phys Oceanogr **10**:1499-1508

Berthot A, Pattiaratchi C (2006) Mechanisms for the formation of headland-associated linear sandbanks. Cont Shelf Res **26**: 987-1004

Burgess SC, Kingsford MJ, Black KP (2007) Influence of tidal eddies and wind on the distribution of presettlement fishes around One Tree Island, Great Barrier Reef. Mar Ecol Prog Ser **341**:233-242

Conlon C (1981) Dynamics of flow in the region of the Tsugaru Strait. Louisiana State University, Tech Rep 312

Cushman-Roisin B (1994) Introduction to Geophysical Fluid Dynamics. Prentice Hall, Englewood Cliffs, New Jersey, 320 p

Doos K, Nycander J, Sigray P (2004) Slope-dependent friction in a barotropic model. J Geophys Res **109**:C01008. doi:10.1029/2002JC001517

Guo X, Futamura A, Takeoka H (2004) Residual currents in a semienclosed bay of the Seto Inland Sea, Japan. Geophys Res Lett **109**:C12008. doi:10.1029/2003JC002203

Hatayama T, Awaji T, Akitomo K (1996) Tidal currents in the Indonesian Seas and their effect on transport and mixing. J Geophys Res **101**(C5):12353-12373

Imasato N (1983) What is tide-induced residual current? J Phys Oceanogr **13**:1307-1317

Isoda Y, Baba K (1998) Tides and tidal currents in the Tsugaru Strait. Bull Fish Sci Hokkaido Univ **49**(3):117-130

Ito T, Togawa O, Ohnishi M, Isoda Y, Nakayama T, Shima S, Kuroda H, Iwahashi M, Sato C (2003) Variation of velocity and volume transport of the Tsugaru Warm Current in the winter of 1999-2000. Geophys Res Lett **30**(13):1678. doi:10.1029/2003GL017522

Japan Coast Guard (1992) Tidal Harmonic Constants Tables Japanese Coast. Tech Rep 742

Kuroda H, Isoda Y, Ohnishi M, Iwahashi M, Satoh C, Nakayama T, Ito T, Iseda K, Nishizawa K, Shima S, Togawa O (2004) Examination of harmonic analysis methods using semi-regular sampling data from an ADCP installed on a regular ferry. Oceanogr Japan **13**(6):553-564

Li C (2006) Modeling of bathymetry-locked residual eddies in well-mixed tidal channels with arbitrary depth variations. J Phys Oceanogr **36**:1974-1993

Maddock L, Pingree RD (1978) Numerical simulation of the Portland tidal eddies. Estuar Coast Mar Sci **6**:353-363

Matsumoto K, Takanezawa T, Ooe M (2000) Ocean tide models developed by assimilating TOPEX/POSEIDON altimeter data into hydrodynamical model: a global model and a regional model around Japan. J Oceanogr **56**:567-581

Maze R, Langlois G, Grosjean F (1998) Tidal Eulerian residual currents over a slope, analytical and numerical frictionless models. J Phys Oceanogr **28**:1321-1332

Na H, Isoda Y, Kim K, Kim YH, Lyu SJ (2009) Recent observations in the straits of the East/Japan Sea, A review of hydrography, currents and volume transports. J Mar Syst **78**:200-205

Nakamura T, Awaji T, Hatayama T, Akitomo K, Takizawa T (2000) Tidal exchange through the Kuril Straits. J Phys Oceanogr **30**:1622-1644

Nihoul JC, Hecq J (1984) Influence of the residual circulation on the physico-chemical characteristics of water masses and the dynamics of ecosystems in the Belgian coastal zone. Cont Shelf Res **3**(2):167-174

Odamaki M (1984) Tide and tidal current in the Tsugaru Strait. Bull Coast Oceanogr **22**(1):12-22

Ogura S (1932) The tide of Tsugaru Strait. Hydrogr Bull **110**:1-26

Onishi M, Ohtani K (1997) Volume transport of the Tsushima Warm Current, west of Tsugaru Strait bifurcation area. J Oceanogr **53**:27-34

Onishi M, Isoda Y, Kuroda H, Iwahashi M, Satoh C, Nakayama T, Ito T, Iseda K, Nishizawa K, Shima S, Togawa O (2004) Winter transport and tidal current in the Tsugaru Strait. Bull Fish Sci Hokkaido Univ **55**(2):105-119

Oonishi Y (1977) A numerical study on the tidal residual flow. J Oceanogr Soc Japan **33**:207-218

Park MJ, Wang DP (2000) Tidal vorticity around a coastal promontory. J Oceanogr **56**:261-273

Pingree R (1978) The formation of the Shambles and other banks by tidal stirring of the seas. J Mar Biol Ass UK **58**:211-226

Pingree R, Maddock L (1979) The tidal physics of headland flows and offshore tidal bank formation. Mar Geol **32**:269-289

Pugh DT (1987) Tides, surges, and mean sea-level. John Wiley and Sons, 472 p

Ridderinkhof H (1989) Tidal and residual flows in the Western Dutch Wadden Sea III, Vorticity balances. Neth J Sea Res **24**(1):9-26

Ro YJ, Jun WS, Jung KY, Eom HM (2007). Numerical modeling of tide and tidal current in the Kangjin Bay, South Sea, Korea. Ocean Sci J **41**(3):153-163

Robinson I (1981) Tidal vorticity and residual circulation. Deep-Sea Res **28A**(3):195-212

Schiller A (2004) Effects of explicit tidal forcing in an OGCM on the water-mass structure and circulation in the Indonesian throughflow region. Ocean Model **6**:31-49

Schiller A, Fiedler R (2007) Explicit tidal forcing in an ocean

general circulation model. Geophys Res Lett **34**:L03611. doi:10.1029/2006GL028363

Schwiderski EW (1980) On charting global ocean tides. Rev Geophys Space Phys **18**(1):243-268

Signell RP, Harris CK (2000) Modeling sand bank formation around tidal headlands. In: 6th International Conference of ASCE, New Orleans, LA, 3-5 Nov 1999, pp 209-222

Talley LD, Min DH, Lobanov VB, Luchin VA, Ponomarev VI, Salyuk AN, Shcherbina AY, Tishchenko PY, Zhabin I (2006) Japan/East Sea water masses and their relation to the sea's circulation. Oceanogr **19**(3):32-49

Tee K (1977) Tide-induced residual current - Verification of a numerical model. J Phys Oceanogr **7**:396-402

Toba Y, Tomizawa K, Kurasawa Y, Hanawa K (1982) Seasonal and year-to-year variability of the Tsushima-Tsugaru Warm Current system with its possible cause. La Mer **20**:41-51

Toyoda T, Awaji T, Ishikawa Y, Nakamura T (2004) Preconditioning of winter mixed layer in the formation of North Pacific eastern subtropical mode water. Geophys Res Lett **31**:L17206. doi:10.1029/2004GL020677

Tsujino H, Motoi T, Ishikawa I, Hirabara M, Nakano H, Yamanaka G, Yasuda T, Ishizaki H (2010) Reference Manual for the Meteorological Research Institute Community Ocean Model (MRI.COM) version 3. Tech Rep 59

Weatherly GL (1972) A study of the bottom boundary layer of the Florida current. J Phys Oceanogr **2**:54-72

Yasuda H (1980) Generating mechanism of the tidal residual current due to the coastal boundary layer. J Oceanogr Soc Japan **35**:241-252

Zimmerman J (1979) On the Euler-Lagrange transformation and the Stokes' drift in the presence of oscillatory and residual currents. Deep-Sea Res **26A**:505-520

Zimmerman J (1981) Dynamics, diffusion and geomorphological significance of tidal residual eddies. Nature **290**:549-555

Appendix A

Vertically Averaged Advective And Viscous Terms

Assuming the hydrostatic approximation, the horizontal momentum equations of the model are given by

$$\frac{\partial u}{\partial t} - fv = -\frac{1}{\rho_0 a\cos\varphi}\frac{\partial p}{\partial \lambda} + a_u + d_u = 0 \tag{A1}$$

$$\frac{\partial v}{\partial t} - fu = -\frac{1}{\rho_0 a}\frac{\partial p}{\partial \varphi} + a_v + d_v = 0 \tag{A2}$$

where a_u, a_v are the three-dimensional advective terms given as

$$a_u = \frac{u}{a\cos\varphi}\frac{\partial u}{\partial \lambda} + \frac{v}{a}\frac{\partial u}{\partial \varphi} + w\frac{\partial u}{\partial z} - \frac{uv\tan\varphi}{a} \tag{A3}$$

$$a_V = \frac{u}{a\cos\varphi}\frac{\partial V}{\partial \lambda} + \frac{v}{a}\frac{\partial V}{\partial \varphi} + w\frac{\partial V}{\partial z} - \frac{v^2\tan\varphi}{a} \tag{A4}$$

where u, v are horizontal velocity components in the λ and φ directions, respectively; w is a vertical velocity component; and d_u, d_v are viscous terms derived from

$$d_u = \frac{1}{a\cos\varphi}\frac{\partial(v_H d_T)}{\partial \lambda} + \frac{1}{a^2\cos\varphi}\frac{\partial(v_H d_S\cos^2\varphi)}{\partial \varphi} + \frac{\partial}{\partial z}\left(v_V\frac{\partial u}{\partial z}\right) \tag{A5}$$

$$d_v = \frac{1}{a\cos\varphi}\frac{\partial(v_H d_S)}{\partial \lambda} + \frac{1}{a^2\cos\varphi}\frac{\partial(v_H d_T\cos^2\varphi)}{\partial \varphi} + \frac{\partial}{\partial z}\left(v_V\frac{\partial v}{\partial z}\right) \tag{A6}$$

In the above equations, v_H and v_V are the horizontal and vertical viscous coefficients, respectively. The horizontal tension d_T and the horizontal shear d_S are obtained from the following equations:

$$d_T = \frac{1}{a\cos\varphi}\frac{\partial u}{\partial \lambda} - \frac{1}{a}\frac{\partial v}{\partial \varphi} \tag{A7}$$

$$d_S = \frac{1}{a\cos\varphi}\frac{\partial v}{\partial \lambda} - \frac{1}{a}\frac{\partial u}{\partial \varphi} \tag{A8}$$

We use the Smagorinsky parameterization (Tsujino et al. 2010) for horizontal viscosity as

$$v_H = \left(\frac{C_H\Delta_{min}^2}{2\sqrt{2}\pi}\right)\sqrt{d_T^2 + d_S^2} \tag{A9}$$

where $\Delta_{\min}$ is the smaller value of longitudinal and latitudinal grid spacings, and C_H is a dimensionless scaling parameter which is set to 2.0 for stable simulation.

In the barotropic mode, the vertically averaged terms X in Eq. (2) and Y in Eq. (3) in momentum equations are defined as

$$X = \int_{-H}^{\eta}(a_u + d_u)dz \tag{A10}$$

$$Y = \int_{-H}^{\eta}(a_v + d_v)dz \tag{A11}$$